



RESEARCH ARTICLE

10.1029/2024JD042109

Key Points:

- The Unified Model with interactive aerosols underestimates total aerosol number by an order of magnitude in a coastal Antarctic case study
- Compared with observations, modeled cloud water is 32 per cent too low and downwelling surface shortwave radiation 76 per cent too high
- Tests show that the cloud biases are largely caused by model meteorology and less affected by the cloud microphysical model processes

Supporting Information:

Supporting Information may be found in the online version of this article.

Correspondence to:

R. Price,
ruthpr@bas.ac.uk

Citation:

Price, R., Orr, A., Field, P. F., Mace, G., & Protat, A. (2025). Simulation of cloud processes over offshore coastal Antarctica using the high-resolution regional UK Met Office Unified Model with interactive aerosols. *Journal of Geophysical Research: Atmospheres*, 130, e2024JD042109. <https://doi.org/10.1029/2024JD042109>

Received 31 JUL 2024

Accepted 21 JAN 2025

Author Contributions:

Conceptualization: R. Price, A. Orr, P. F. Field

Data curation: R. Price, G. Mace, A. Protat

Formal analysis: R. Price, A. Orr, P. F. Field

Funding acquisition: A. Orr

Methodology: R. Price, A. Orr, P. F. Field, G. Mace, A. Protat

Project administration: A. Orr






Software: R. Price, P. F. Field

Supervision: A. Orr, P. F. Field

Visualization: R. Price

Writing – original draft: R. Price

Simulation of Cloud Processes Over Offshore Coastal Antarctica Using the High-Resolution Regional UK Met Office Unified Model With Interactive Aerosols

R. Price¹ , A. Orr¹ , P. F. Field^{2,3} , G. Mace⁴ , and A. Protat^{5,6} 

¹British Antarctic Survey, Cambridge, UK, ²Met Office, Exeter, UK, ³School of Earth and Environment, University of Leeds, Leeds, UK, ⁴University of Utah, Salt Lake City, UT, USA, ⁵Bureau of Meteorology, Melbourne, VIC, Australia, ⁶Australian Antarctic Program Partnership, Institute of Marine and Antarctic Studies, University of Tasmania, Hobart, TAM, Australia

Abstract The Southern Ocean and offshore coastal Antarctica are key regions for global climate. Low level mixed-phase clouds strongly control the surface radiation budget of this region but remain challenging for climate models because of the complex processes controlling the sources and sinks of cloud liquid water, including both cloud liquid water and ice crystals. Here, we examine these interactions using the Unified Model (UM) regional climate model, with the Cloud AeroSol Interacting Microphysics (CASIM) and UK Chemistry and Aerosol (UKCA) models included for interactive aerosol and cloud microphysics. We simulate two case studies from the second field campaign of Clouds Aerosols Precipitation Radiation and atmospheric Composition over the Southern Ocean Phase 2 (CAPRICORN-2), which represent the open ocean and the offshore coastal region of Antarctica. Compared with these observations, we find that the UM underestimates surface aerosol concentration by up to an order of magnitude and investigate the effect of this bias on the simulated cloud microphysical and radiative properties. We find that the cloud liquid water path (LWP) and surface radiative fluxes are also biased in the offshore coastal Antarctic case study, with a 32% mean underestimation of LWP and 76% mean overestimation of downwelling surface shortwave flux. Sensitivity tests show that the cloud liquid water bias is largely caused by deficiencies in the representation of the meteorology, and less by aerosol or cloud microphysical properties. Our results provide key insights on the modeling of cloud processes in high southern latitudes.

Plain Language Summary The Southern Ocean and coastal Antarctica are crucial for global climate. Low-level clouds made of a mix of water droplets and ice crystals play a significant role in controlling the amount of radiation that reaches the surface in this area. However, these clouds are difficult to accurately simulate in climate models due to the complex interactions between the water and ice in them. In this study, we use a regional climate model with state-of-the-art cloud and aerosol microphysics to better understand these interactions. We simulate specific cases from the CAPRICORN-2 field campaign, which studied clouds, aerosols, precipitation, radiation, and atmospheric composition over the Southern Ocean. Our findings show that the UM model underestimates the concentration of aerosols at the surface by up to 10 times compared with actual observations. We explore how this inaccuracy affects the simulated cloud properties and the radiation reaching the surface. Further tests reveal that the main reason for errors in simulated liquid water clouds is due to the incorrect representation of weather conditions in the model, rather than issues with aerosols or cloud properties. Our results highlight important areas for improvement in modeling cloud processes in the high southern latitudes.

1. Introduction

Southern Ocean clouds have global importance in the climate system (Kang et al., 2023; Williams et al., 2023). The presence and microphysical structure of clouds over the Southern Ocean are important factors in the local energy budget, because of for example, the large difference in albedo between the ocean surface and overlying clouds (Fitzpatrick & Warren, 2007). Despite their importance, clouds over the Southern Ocean have typically been poorly represented in climate or weather models (Lang et al., 2021; Protat et al., 2017; Stanford et al., 2023). For example, models have been shown to have too much incoming shortwave (SW) radiation over the Southern Ocean (Cesana et al., 2022), with associated impacts on ocean heat uptake (Morrison et al., 2022; Trenberth & Fasullo, 2010), sea ice, and atmospheric energy transport (Ceppi et al., 2012; Kay et al., 2016). Moreover, the

© 2025. The Author(s).

This is an open access article under the terms of the [Creative Commons Attribution License](https://creativecommons.org/licenses/by/4.0/), which permits use, distribution and reproduction in any medium, provided the original work is properly cited.

Writing – review & editing: R. Price,
A. Orr, P. F. Field, G. Mace, A. Protat

clouds over the Southern Ocean influence the equilibrium climate sensitivity, a key metric for the understanding and prediction of the global climate response to anthropogenic forcing (Bodas-Salcedo et al., 2019; Zelinka et al., 2020).

Previous regional modeling studies of polar mixed-phase clouds have highlighted the importance of the representation of cloud microphysics in models. Liquid water formation can be suppressed by the presence of ice crystals due to the Wegener-Bergeron-Findeisen process, making cloud liquid water content susceptible to parameterized microphysical processes governing the rate of ice crystal formation and growth. Such processes include riming (Furtado & Field, 2017; Gilbert et al., 2020), vapor deposition (Furtado & Field, 2017), secondary ice formation (Young et al., 2019), raindrop freezing (Vignon et al., 2021), and especially the parameterization of ice nucleation itself (Furtado & Field, 2017; Vergara-Temprado et al., 2018; Vignon et al., 2021). However, the representation of meteorological fields and boundary layer dynamics can also be important. For example, in a regional modeling case study of Arctic clouds, McCusker et al. (2023) showed that biases in the meteorological fields used to force the model caused biases in the representation of clouds, which consequently impacted the surface temperature. Furtado and Field (2017) showed that the mixing of ice due to sub-grid scale turbulence has a significant effect on the amount, phase, and vertical distribution of cloud water in simulations of a Southern Ocean cyclone. Cloud top turbulence has also been shown to be a critical process for models to accurately represent in order to form and maintain mixed-phase clouds (Furtado et al., 2016; Gilbert et al., 2020; Vignon et al., 2021). Model vertical resolution also plays a role because of the importance of resolving the sharp gradients in moisture and temperature that can drive these cloud top processes (Barrett et al., 2017; Vignon et al., 2021). Taken together, these results show that relatively high horizontal and vertical resolution, accurate input data, and a high level of sophistication in cloud microphysical, boundary layer, and cloud re fraction processes are required for accurate simulations of mixed-phase clouds in the polar regions.

Recent observational campaigns have provided novel insights into the abundance, composition, and behavior of aerosols in the Southern Ocean and Antarctica. Primary production from sea spray and secondary production from biogenic vapors are the key local sources of aerosols in the Southern Ocean during summer (Schmale et al., 2019). Measurements from four ship and aircraft field campaigns in the Southern Ocean between 2016 and 2018 are summarized in McFarquhar et al. (2021), which include the Clouds Aerosols Precipitation Radiation and atmospheric Composition over the Southern Ocean Phase 2 (CAPRICORN-2) campaign. These results indicate a pristine environment with low concentrations of ice nucleating particles (INPs). They also present evidence that new particle formation (gas-to-particle formation of aerosols in the atmosphere) above cloud dominates over long-range transport of aerosols, something that has been shown in other observational studies (McCoy et al., 2021). Moreover, the results given by McFarquhar et al. (2021) show high variability in cloud condensation nuclei (CCN) and cloud droplet number concentration (CDNC) even for similar cloud regimes, showing that the influence of aerosols on clouds cannot be treated in isolation from dynamical and boundary layer processes. Moreover, the Southern Ocean is a valuable “natural laboratory” to study aerosol processes typical of the pre-industrial period (Carslaw et al., 2013; Regayre et al., 2020). For example, Revell et al. (2019) studied Southern Ocean aerosols in the HadGEM3-GA7.1 global chemistry-climate model and found that using in situ measurements to constrain the sea spray source function and dimethylsulphide (DMS) chemistry scheme can improve the representation of aerosol optical depth, CCN concentration, and CDNC. However, less attention has been given to aerosols in high-resolution, regional model case studies where cloud microphysics is better resolved.

The UK Chemistry and Aerosol model (UKCA) has recently been coupled to the Cloud AeroSol Interacting Microphysics model (CASIM) in the regional climate configuration of the UK Met Office (UKMO) Unified Model (UM) (Gordon, et al., 2020, 2023). This configuration of the UM with UKCA and CASIM provides a state-of-the-art tool for the simulation of aerosol-cloud interactions. In this study, we use the UM with UKCA and CASIM to run high-resolution (approximately 2 km, i.e., cloud resolving) simulations of two case studies representing contrasting conditions experienced by the CAPRICORN-2 campaign over the open Southern Ocean and offshore coastal Antarctica. This is the first time that this model configuration has been tested in these regions. In particular, we investigate the respective importance of meteorology and aerosol controls for accurate cloud simulations. We also use the model to examine the observed difference in aerosol sources between the sea spray-dominated open ocean and the more biologically active Antarctic coast. We evaluate the simulated aerosols in these two regimes/regions against the CAPRICORN-2 measurements and then investigate the effect of the aerosols on clouds and surface radiative fluxes in the model. Since the CAPRICORN-2 data show a potential link

between biogenic aerosols and cloud properties near the Antarctic coast, we are particularly interested in evaluating the model aerosol-cloud interactions for the coastal Antarctica case study. The model and simulations are presented in Section 2, as well as details of the observational data sets used. Results are presented in Section 3 and their implications discussed in Section 4. Section 5 is a conclusion.

2. Materials and Methods

2.1. Observational Data Sets

2.1.1. CAPRICORN-2

The CAPRICORN-2 campaign took place on board the Research Vessel (R/V) *Investigator* in January and February 2018, in the Australian sector of the Southern Ocean. A full description of the campaign and the instruments deployed is given in McFarquhar et al. (2021) and Mace et al. (2021). In this study, we have used ship-based measurements of: (a) Downwelling longwave (LW) and SW radiative fluxes from pyranometer and pyrgeometer, (b) aerosol concentrations from condensation particle counter (Humphries et al., 2020), and (c) cloud mask, liquid water path (LWP), and CDNC from cloud radar, lidar, and microwave radiometer (Mace et al. (2021)). The condensation particle counter was situated on the *Investigator* and measured the number concentration of particles greater than 10 nm diameter (N_{10}) at a time resolution of 1 s. The data set we use consists of hourly averages that have been computed following quality control and data filtering. The uncertainty of the measurements is less than 3%. We also use potential temperature profiles measured by five radiosondes that were launched from the ship at times between 00:53 and 01:05 UTC.

2.1.2. Advanced Microwave Scanning Radiometer 2

The Advanced Microwave Scanning Radiometer 2 (AMSR2) sensor is on board the Global Change Observation Mission-Water 1 (GCOM-W1) satellite (Imaoka et al., 2010). It provides twice daily overpasses to measure microwave emissions of the surface and atmosphere. In this study, we have used the daily ascending and descending AMSR2 measurements of LWP. The LWP measurements have a root mean square accuracy of 25 g m^{-2} (Wentz, 1997). Additional systematic error from assumptions in the partitioning of cloud and rain can potentially reach approximately 5% over the Southern Ocean (O'Dell et al., 2008). The AMSR2 measurements are available on a $0.25^\circ \times 0.25^\circ$ latitude-longitude grid.

2.2. Models and Simulations

2.2.1. Unified Model

The UM is an atmospheric model that can be used in either a global climate or regional configuration. Here, we have used the Regional Atmosphere Land version 3.1 (RAL3.1), which includes CASIM (Field et al., 2023), coupled to UKCA (O'Connor et al., 2014) for the simulation of aerosol-cloud interactions. The RAL3.1 configuration is based on the RAL3 configuration, which is the latest operational configuration of the UM. The main changes from the previous configurations (RAL2, Bush et al., 2023) to RAL3 are the change of cloud microphysics to a double moment implementation of CASIM (Field et al., 2023) and the cloud fraction scheme to bimodal (Van Weverberg et al., 2021). Boundary layer turbulence is parameterized using the “blended” approach of Boutle et al. (2014), which combines the Lock et al. (2000) scheme (suitable for relatively lower resolutions) and the Smagorinsky (1963) (suitable for relatively higher resolutions). See Bush et al. (2023) for more details. At the grid resolutions used in this study (approximately 2 km), the convective parameterization is switched off and convective mixing is handled explicitly by the model. CASIM simulates the number and mass of liquid and frozen hydrometeors in five different classes. It also simulates cloud microphysical processes such as condensation, sedimentation, autoconversion to rain, riming, homo- and heterogeneous freezing, sublimation, and depositional growth. It has been previously evaluated against observations (Grosvenor et al., 2017), including by Vergara-Temprado et al. (2018) in the Southern Ocean against satellite observations, where it was shown that the more accurate treatment of ice microphysics by CASIM improved the simulation of cloud radiative properties. The bimodal cloud fraction scheme uses sub-grid vertical velocity variance diagnosed from the UM (that acts to broaden the sub-grid saturation distribution) and the ice particle population (that narrows the sub-grid saturation distribution) to determine the resultant sub-grid humidity distribution. This distribution is combined with temperature and pressure information to compute the amount of condensed liquid water and liquid cloud fraction that

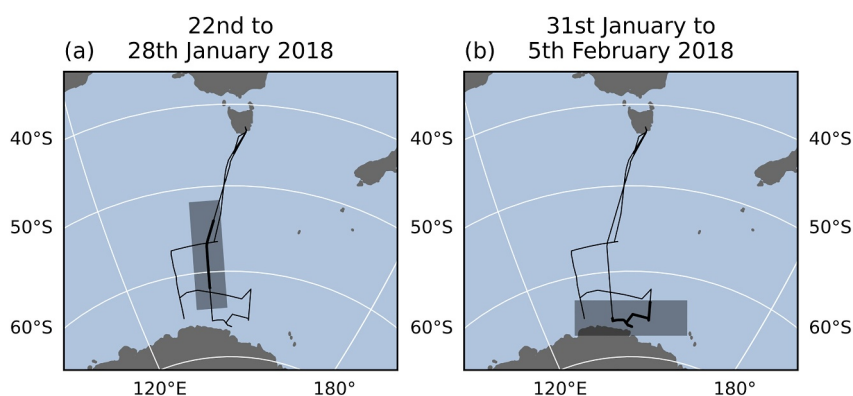


Figure 1. Maps showing the CAPRICORN-2 ship track (black lines) and Unified Model domains (shaded black boxes) for (a) the ocean case study from 22nd January 2018 to 28th January 2018 and (b) the coastal case study from 31st January 2018 to 5th February 2018. The thick black line in each domain indicates position of R/V *Investigator* during each simulation.

exists in a grid box. Specifically, the UM with CASIM uses a saturation adjustment approach for liquid condensation, where vapor exceeding the liquid saturation threshold within a grid cell is condensed instantaneously at each timestep. This approach, which typically operates on a 60 s timestep in the UM, avoids the need for a prognostic treatment of liquid supersaturation that would otherwise be necessary for shorter (~ 2 s) liquid cloud adjustment timescales (Field et al., 2023; Gordon et al., 2020).

UKCA uses the GLObal Model of Aerosol Processes (GLOMAP-Mode) to simulate aerosol number and mass in four soluble log-normal size modes and one insoluble mode. The aerosol species it simulates are sulfate, black carbon, organic carbon, and sea salt, with each size mode assumed to be an internal mixture of mass components. Dust aerosol is not included in the configuration of UKCA used here, but dust mass is taken from climatological values as in Field et al. (2023). Aerosol processes simulated by GLOMAP-Mode include primary emissions, secondary formation, growth by condensation or coagulation, dry and wet deposition, scavenging within and below clouds, and aqueous formation of sulfate in cloud droplets. The coupling of UKCA and CASIM is described by Field et al. (2023) and Gordon et al. (2020, 2023). The size distribution and composition of aerosols from UKCA is passed to CASIM, which then uses the Abdul-Razzak and Ghan (2000) aerosol activation parameterization to diagnose the number of CCN and calculate the CDNC. The number and size of droplets in liquid-containing clouds are then used within the UM for the calculation of radiation fluxes and precipitation. In this way, the coupling of UKCA and CASIM creates a state-of-the-art tool for the simulation of aerosol-cloud interactions and their role in regional climate systems. As mentioned above, the UM with CASIM has been assessed in the Southern Ocean before, but here we apply the UM coupled to CASIM and UKCA over this region for the first time to assess its representation of aerosol-cloud interactions.

2.2.2. UM Simulations

The UM model is used to simulate case studies representing the open ocean from 22nd to 28th January 2018 and offshore coastal Antarctica from 31st January to 5th February 2018 at 0.018° (approximately 2 km) horizontal resolution. These are hereafter referred to as the ocean case study and coastal case study, respectively. They are simulated over two separate domains, shown in Figure 1. The simulations for each case study are run using a frequent re-initialization approach similar to that used in Hansen et al. (2023) and described in Gordon et al. (2020), which consists of running daily 36-hr forecasts initialized at 00Z, with the initial 12-hr period treated as spin-up and discarded to create a continuous time series from all forecasts. The model is driven by output from forecasts of the global configuration of the UM simulation on a $0.83^\circ \times 0.55^\circ$ latitude-longitude grid (i.e., N216, equivalent to ~ 60 km resolution at the equator). The initial meteorological fields for the global driving model are taken from operational UKMO analysis for the appropriate day and the global model is reinitialized every 36 hr in the same way as the high-resolution nest. The initial conditions for the aerosol fields are taken from output of the global coupled UK Earth System Model and spun-up for a period of 2 weeks prior to the first forecast of each domain. Note therefore that the aerosols are not reinitialized during the forecasts because the aerosol fields are not available on 24 hr intervals to use as initial conditions. Instead, the aerosol fields from one forecast are carried

Table 1
List of Unified Model Simulations

Simulation	Description
CONTROL	UM coupled to UKCA and CASIM
FIXED_DROP	CONTROL + prescribed CDNC value of 150 cm^{-3}
ICE_MICROPHYS	CONTROL + Heterogeneous raindrop freezing switched off, Hallett Mossop secondary ice production switched off, and the temperature threshold for the nucleation of ice lowered from -8°C to -25°C
ERA5_INITIAL	CONTROL + Initialization of simulations using ERA5 meteorological fields
MIXING	CONTROL + Enhanced vertical mixing of air from surface in the boundary layer
ALL_TESTS	CONTROL + FIXED_DROP + ICE_MICROPHYS + ERA5_INITIAL + MIXING

over to the next one at the reinitialization stage. This procedure is described in Gordon et al. (2020). These simulations (using the standard RAL3.1 configuration) are subsequently referred to as CONTROL.

Because we are interested in assessing the model behavior with regard to secondary aerosol and aerosol-cloud interactions in the biologically active region in the coastal case study, we also ran five additional sensitivity tests for the offshore coastal Antarctica case study only. These tests target the relative effects of aerosols and meteorology on the simulation of clouds and are summarized in Table 1. First, in simulation CONTROL, CDNC is calculated interactively from the UKCA aerosol fields and UM meteorology. To test the effects of this interactive droplet activation on the simulated cloud microphysics and radiation, we also ran a simulation with a prescribed CDNC of 150 cm^{-3} , referred to as simulation FIXED_DROP. The value of 150 cm^{-3} was chosen because it roughly corresponds to the values of CDNC that were measured during the two case studies. Second, we perturbed several processes in CASIM relating to the formation of cloud ice at the expense of liquid, referred to as simulation ICE_MICROPHYS. This involved: (a) lowering the temperature threshold for ice formation in the ice nucleation parametrization from -8°C to -25°C to suppress ice formation, (b) switching off secondary ice formation via the Hallett Mossop process and the raindrop freezing process, and (c) converting all cloud water advected into the high-resolution domain from the lateral boundary conditions (i.e., from the global configuration of the UM) to liquid to further reduce the loss of vapor and liquid water to existing ice crystals. Third, in simulation ERA5_INITIAL, the global configuration of the UM was initialized from meteorological fields from the European Center for Medium-range Weather Forecasts Reanalysis version 5 (ERA5, Hersbach et al., 2020) instead of the default UKMO analysis. Fourth, in simulation MIXING the calculation of the height at which convective mixing takes over from boundary layer mixing was changed to promote more turbulent mixing in the boundary layer. Here, the presence of convection is diagnosed empirically according to model humidity gradients in the boundary layer, which in turn influences the calculation of the vertical extent of parameterized turbulent mixing. Since the convective scheme is switched off in this model configuration, the boundary layer mixing is more efficient than convective mixing in our simulations. The humidity gradient threshold for the presence of convection in a model layer was increased by a factor of approximately 1.8. This change was therefore designed to promote enhanced vertical mixing of air in the boundary layer, to promote more transport of water vapor from the surface up to cloud level relative to CONTROL. This approach enables us to investigate the effect of sub-grid variability in vapor sources and sinks on cloud water condensation and evaporation without altering aerosol or ice phase processes directly. Fifth, simulation ALL_TESTS includes all the above sensitivity tests in one simulation.

Outputs from the simulations are subsequently compared with the observational data sets. To compare model outputs with the CAPRICORN-2 measurements, we compute hourly means from the high-time resolution measurements of LWP, CDNC, and surface radiative fluxes, that is, to reduce noise. These are compared with instantaneous spatial means of collocated model output from a three-by-three grid of (2 km) model grid boxes, where the middle grid box contains the location of the ship. The 1 hr window for the temporal average of the measurements approximately corresponds to the time it would take to advect an air parcel across these three-by-three grid boxes for wind speeds experienced during each case study (not shown), that is, aiding the comparison between point-based observations and model output, following the approach described in Illingworth et al. (2007). Model CDNC values shown are the in-cloud median throughout the column. Vertical profiles of

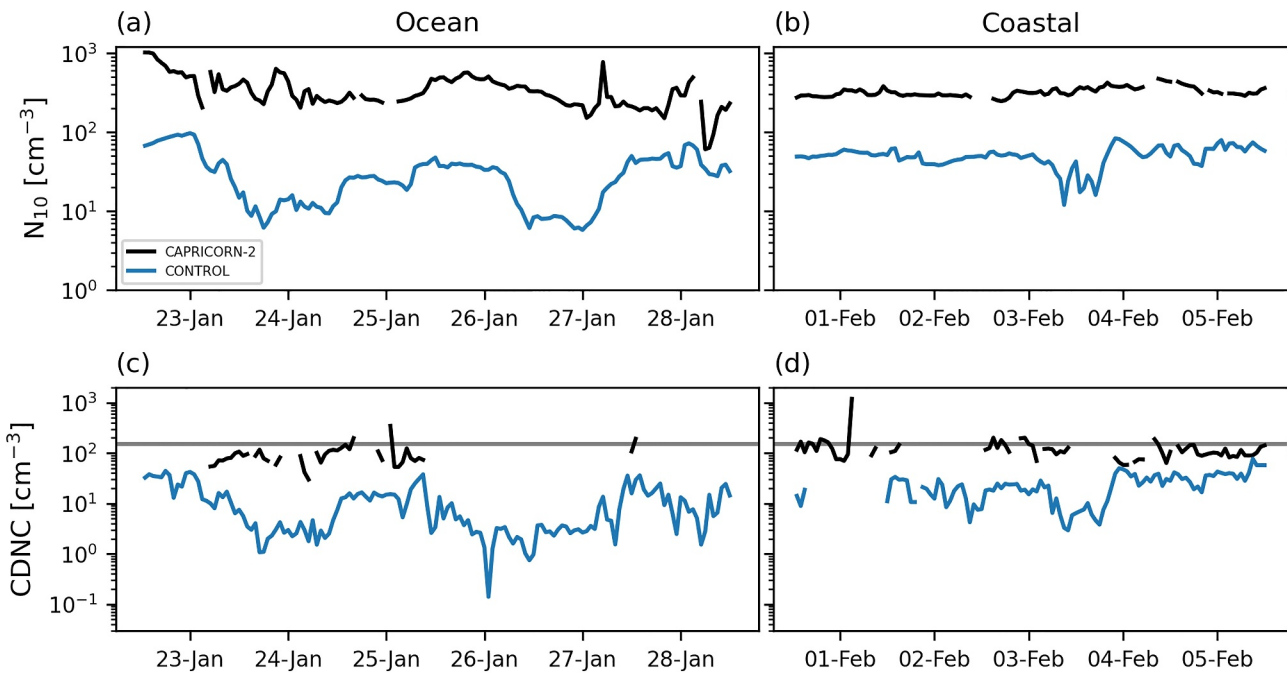


Figure 2. Time series of (a, b) N_{10} (concentration of particles larger than 10 nm) from condensation particle counter measurements (black) and (c, d) cloud droplet number concentration (CDNC) retrieved from Lidar, radar, and microwave radiometer (black) and output from CONTROL simulations (blue). Measurements are hourly averaged data, model output is hourly instantaneous data averaged over nine gridpoints nearest to the R/V *Investigator*. Results from the ocean case study (22nd January 2018–28th January 2018) are in panels (a, c), and from the coastal case study (31st January 2018–5th February 2018) in panels (b, d). Gaps in the CAPRICORN-2 time series correspond to periods where measurement retrievals are not valid. Gaps in the CONTROL time series in panels (c, d) are where the model does not simulate any liquid clouds. Horizontal lines on panels (c, d) show the value used for prescribed CDNC in simulation FIXED_DROP.

simulated potential temperature 1 hour after initialization, as well as profiles from UKMO analysis and ERA5 reanalysis, are compared to data from the five radiosonde profiles. To compare model output and AMSR2 measurements, we bilinearly interpolate model output to the AMSR2 grid, and select the model timesteps that are closest to the local AMSR2 overpass times. We also apply the land and sea ice mask from AMSR2 to the model output, as AMSR2 LWP measurements are only available over the ocean.

3. Results

3.1. CONTROL Simulation

In this section, we compare output from the CONTROL simulation with measurements made during CAPRICORN-2. Figures 2a and 2b show measurements of particles larger than 10 nm diameter, N_{10} , for each case study. During the ocean case study, the N_{10} concentration is typically between 250 and 600 cm^{-3} , peaking at approximately 1,000 cm^{-3} in the first few hours of the time series, and reaching a minimum of about 50 cm^{-3} at the end. By contrast, the N_{10} concentration during the coastal case study is slightly lower and less variable, varying between about 250 and 500 cm^{-3} . Neither case study has the correct N_{10} concentration simulated in CONTROL. In both domains, the simulated N_{10} concentration is approximately 50 cm^{-3} , that is, corresponding to an underestimation of the measurements by a factor of 5–10. Interestingly, the variability in N_{10} in the ocean case study is somewhat captured by the model, as is the lower variability in the coastal case study (Figure S1 in Supporting Information S1). As is to be expected from the underestimate of N_{10} , the CDNC values are also systematically underestimated in CONTROL for both case studies (Figures 2c and 2d). The measured CDNC values are typically around 200 cm^{-3} , though can vary between about 10 and 1,000 cm^{-3} , while the CONTROL values in both case studies rarely exceed 75 cm^{-3} and are sometimes lower than 1 cm^{-3} . Additionally, CCN concentrations are also underestimated by CONTROL (not shown), which is consistent with the underestimate of N_{10} and CDNC. As discussed in McFarquhar et al. (2021), the CDNC values are somewhat higher in the coastal case study than the ocean case study, which is hypothesized to be because of a biogenic source of aerosols at the coast increasing the number of particles that act as efficient CCN. Alternatively, analysis of the observations on

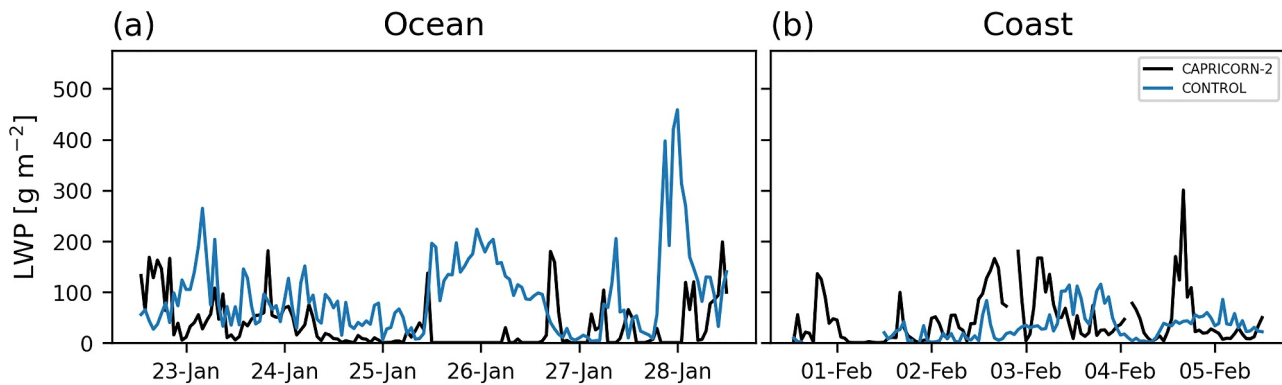


Figure 3. Time series of liquid water path from microwave radiometer measurements (black) and output from CONTROL simulations (blue). Measurements are hourly averaged data and model output is hourly instantaneous data averaged over nine gridpoints nearest to the R/V *Investigator*. Results from the ocean case study (22nd January 2018–28th January 2018) are in panel (a), and from the coastal case study (31st January 2018–5th February 2018) in panel (b). Gaps in time series correspond to periods where the measurement retrievals are not valid or where the model does not simulate any liquid clouds.

4th and 5th February by Mace et al. (2024) is consistent with a free tropospheric source of particles during the time when the air was over the Antarctic continent before reaching the ship. Though the model output also has higher CDNC values in the coastal case study than the ocean, the significant underestimation of N_{10} and CDNC in both domains suggests that the underlying aerosol and cloud activation processes are nonetheless not correctly represented in the model.

We examine the behavior of the liquid clouds in CONTROL by comparing model output with measurements of LWP for both case studies (Figure 3). Note that we focus on LWP because there is a reasonable agreement in the cloud mask between model output and radar and Lidar results (Figures S2 and S3 in Supporting Information S1). The measurements are approximately 50 g m^{-2} on average in both case studies, with the ocean case study reaching maximum values of approximately 200 g m^{-2} and the coastal case study reaching approximately 300 g m^{-2} . In the ocean case study, the model captures the measured LWP time series well between 22nd and 25th January, but overestimates LWP at certain times between 25th and 28th January. In the coastal case study, there are periods where the LWP from CONTROL is too low compared with measurements, and also where CONTROL fails to simulate any liquid clouds at all. For example, at the beginning of the coastal case study between 31st January and 1st February, CONTROL does not simulate any liquid cloud, while the measured LWP values are up to 120 g m^{-2} . Over the entire coastal case study, the CONTROL simulation underestimates the measured LWP by approximately 32%.

Figure 4 shows the downwelling radiative fluxes for the coastal case study, to help explain how they are affected by the effect of the underestimate of simulated LWP for this case study (Figure 3). Compared with the measurements, downwelling SW flux is consistently overestimated by CONTROL by up to 400 W m^{-2} , especially for example, on 2nd and 3rd February. At the beginning of the case study, when CONTROL erroneously simulates clear sky conditions by failing to simulate a liquid layer (between approximately 12:00 UTC on 31st of January and 03:00 UTC on 1st February), downwelling SW is overestimated in the first few hours of daylight on 1st February. During this period, the CONTROL simulation also underestimates the downwelling LW flux by approximately 100 W m^{-2} . The effect of this clear sky model bias during this period is more pronounced in the downwelling LW than the SW because it mostly occurs during night. The downwelling LW flux is also underestimated at other times, by up to 75 W m^{-2} . The total downwelling flux is dominated by the SW bias during daylight hours, with thus a better agreement between measurements and CONTROL during the night despite some underestimation of LW flux by CONTROL.

3.2. Sensitivity Tests

To better understand to what extent the representation of key meteorological processes (i.e., enhanced mixing of water vapor in the boundary layer, meteorological fields used for initialization) or aerosols is causing the underestimate of LWP (and associated radiative biases) in the CONTROL simulation in the coastal case study, this section examines the results from the sensitivity tests conducted with the UM (Table 1). Figure 5 shows

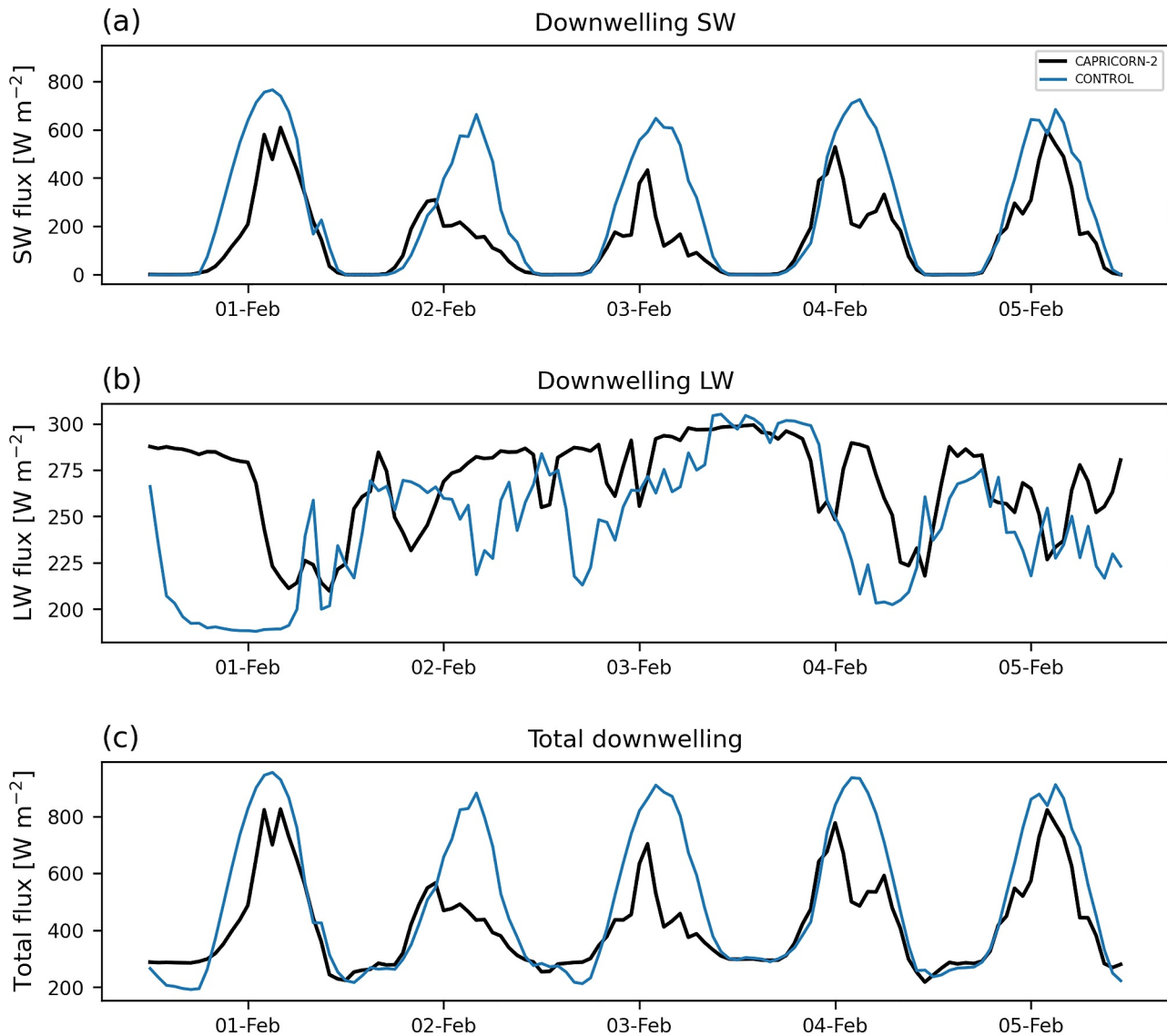


Figure 4. Time series of downwelling (a) SW, (b) LW, and (c) total radiation fluxes from pyranometer and pyrgeometer measurements (black) and output from the CONTROL simulation (blue) for the coastal case study (31st January 2018–5th February 2018). Measurements are hourly averaged data, model output is hourly instantaneous data averaged over nine gridpoints nearest to the R/V *Investigator*.

probability density functions (PDFs) of LWP from CAPRICORN-2, CONTROL, and sensitivity tests for the coastal case study, while Table 2 compares their minimum, maximum, mean, and median values. The time series of LWP, downwelling SW, and downwelling LW from the sensitivity tests are shown in Figures S4–S6 in Supporting Information S1, respectively. The PDF of LWP from the measurements ranges from around 0 to 300 g m^{-2} and has a peak at relatively low values (Figure 5a), which is apparent from its mean value of 46.97 g m^{-2} and median of 26.03 g m^{-2} (Table 2). By contrast, the LWP PDF from the CONTROL simulation overestimates the number of occurrences of small values ($<5 \text{ g m}^{-2}$) and underestimates occurrences at larger values (Figure 5a), which is apparent from its mean value of 31.73 g m^{-2} and maximum value of 115.06 g m^{-2} being considerably less than the measurements (Table 2). However, Figure 5a shows that ALL_TESTS captures the measured PDF of LWP values reasonably well, and much better than CONTROL. For example, the mean value of 46.58 g m^{-2} from ALL_TESTS is around 47% higher than CONTROL, and in excellent agreement with the measurements (Table 2) (though the median value 32.40 g m^{-2} overestimates the measured median). Similarly, the maximum value of 303.02 g m^{-2} from ALL_TESTS is around double that of CONTROL, and also in excellent agreement with the measured value of 300.40 g m^{-2} (Table 2).

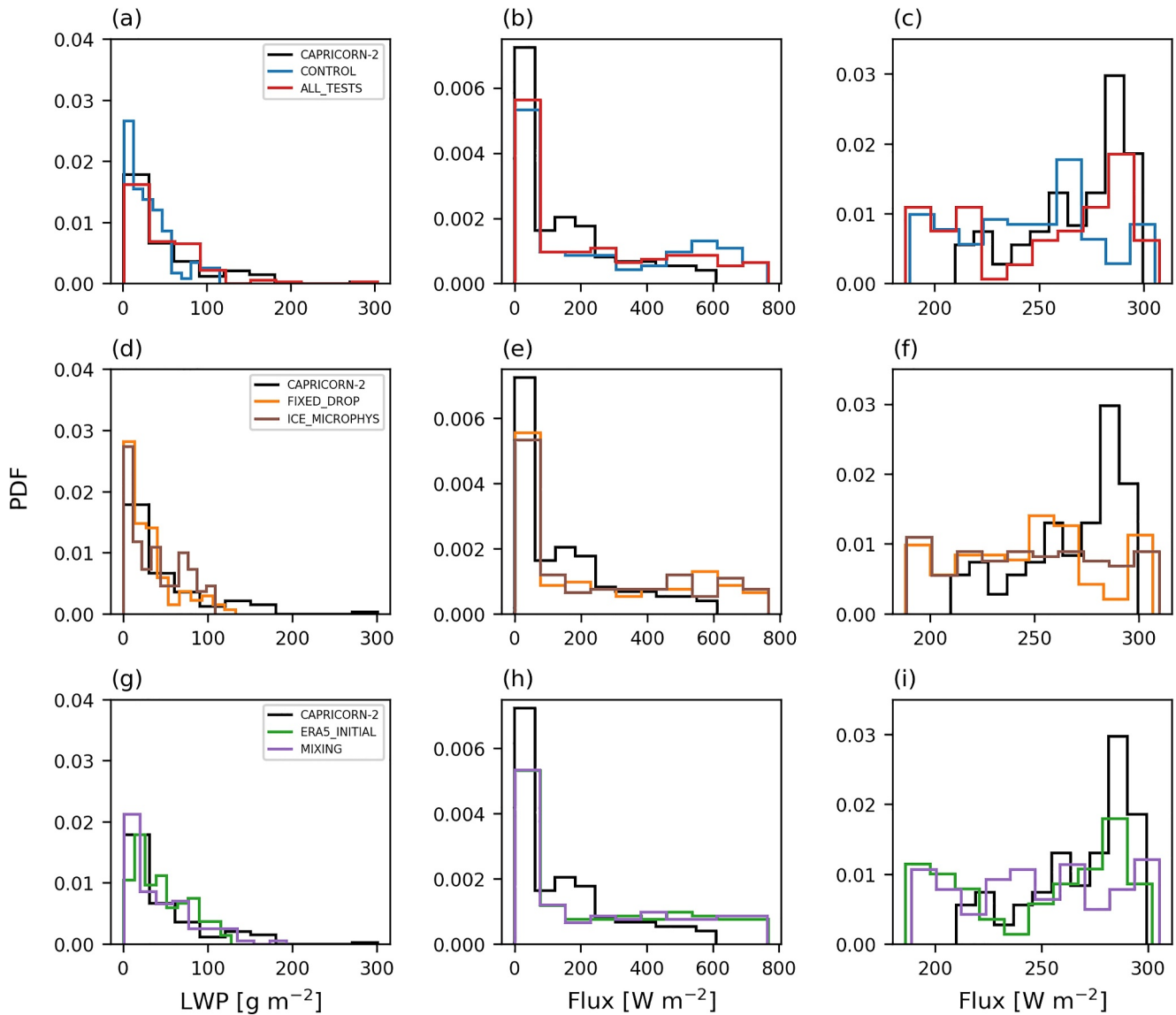


Figure 5. Probable density functions of (a, d, and g) liquid water path, (b, e, and h) downwelling SW flux and (c, f, and i) downwelling LW flux from measurements (black) and output from CONTROL and Unified Model sensitivity tests (colored lines) for the coastal case study. Panels (a–c) show output from the CONTROL and ALL_TESTS simulations, (d–f) show output from the FIXED_DROP and ICE_MICROPHYS simulations, and (g–i) show output from the ERA5_INITIAL and MIXING simulations.

By examining the LWP PDFs of the four other UM sensitivity tests that when combined together form ALL_TESTS (Table 1), we can identify which of them are responsible for the improvement in ALL_TESTS relative to CONTROL. Figure 5d shows LWP PDFs from the tests targeting potential cloud microphysical sink terms of cloud liquid water, which were FIXED_DROP (too strong conversion of cloud liquid to rain) and ICE_MICROPHYS (too much ice formation at the expense of liquid). The LWP PDFs from both these experiments are similar to that of CONTROL, that is, overestimating the number of occurrences of small values and underestimating occurrences at larger values. See also Table 2. This result suggests that neither removal by liquid precipitation nor the Wegener-Bergeron-Findeison process is primarily responsible for the LWP underestimation in this case study. In Figure 5c, PDFs are shown for the sensitivity tests targeting meteorological sources of cloud liquid water (initialization fields in ERA5_INITIAL, and the mixing of water vapor in the low boundary layer in MIXING). The PDFs of LWP from ERA5_INITIAL and MIXING show more differences relative to CONTROL. Both PDFs have fewer occurrences of low LWP and higher maximum LWP values than that of CONTROL, bringing them closer to the shape of ALL_TESTS, though still overestimating the number of occurrences of small

Table 2

Minimum, Maximum, Mean, and Median Values of Liquid Water Path in the Coastal Case Study (31st January 2018–5th February 2018) for Measurements, CONTROL, and Unified Model Sensitivity Tests

	Liquid water path [g m^{-2}]			
	Min.	Max.	Mean	Median
CAPRICORN-2	0.54	300.40	46.97	26.03
CONTROL	0.99	115.06	31.73	26.13
FIXED_DROP	0.27	132.61	30.84	24.19
ICE_MICROPHYS	0.26	108.88	37.85	30.17
ERA5_INITIAL	0.09	127.43	45.88	40.16
MIXING	0.47	192.51	41.02	28.55
ALL_TESTS	1.20	303.02	46.58	32.40

Note. Bold values in each column indicate closest numerical agreement with observed value.

values and underestimating occurrences of larger values relative to the measurements. For example, the mean LWP value for ERA5_INITIAL is 45.88 g m^{-2} (about 45% increase relative to CONTROL) and for MIXING 41.02 g m^{-2} (29% increase), which are broadly in agreement with the ALL_TESTS value of 46.58 g m^{-2} (Table 2). Examination of the time series of LWP (Figure S3 in Supporting Information S1) shows that the better performance of MIXING and ERA5_INITIAL relative to CONTROL is driven by a few short periods where LWP is increased substantially. Furthermore, ALL_TESTS performs the best because it captures the improvements of both ERA5_INITIAL and MIXING at different times, leading to higher average values of LWP than any other sensitivity test (Table 2).

Figure 5 also shows PDFs of surface downwelling SW and LW fluxes from CAPRICORN-2, CONTROL, and sensitivity tests for the coastal case study, while Table 3 compares their mean and median values. The PDF of downwelling SW flux from the measurements has a range of approximately 600 W m^{-2} , with a large peak at relatively low values ($<100 \text{ W m}^{-2}$) (Figure 5b), which is apparent from its mean value of 146.14 W m^{-2} and median of 93.17 W m^{-2} (Table 3). The SW PDF from the CONTROL

simulation has fewer occurrences of SW at relatively low values and higher maximum SW values (765.19 W m^{-2}) than that of the measurements (Figure 5b), which is apparent from the mean value of CONTROL of 257.48 W m^{-2} (Table 3). However, the PDF of SW from ALL_TESTS shows little difference compared to CONTROL (Figure 5b), although the mean and median SW values from ALL_TESTS of 227.59 and 126.76 W m^{-2} (respectively) are closer to the measured values (Table 3). The corresponding PDF of downwelling LW flux from the measurements has a range of around 90 W m^{-2} and a peak at approximately 280 W m^{-2} (Figure 5c), which is apparent from its mean value of 268.22 W m^{-2} (Table 3). The LW PDF from the CONTROL simulation fails to capture the peak that is apparent in the measurements, and also its range of about 115 W m^{-2} is larger than the measurements (Figure 5c), which is apparent from the mean value of CONTROL of 244.69 W m^{-2} (Table 3). However, the PDF of LW from ALL_TESTS shows a better comparison against the measurements compared to CONTROL (Figure 5c). For example, the PDF from ALL_TESTS has the same peak as the measurements at approximately 280 W m^{-2} . Examination of the SW and LW PDFs of the four other UM sensitivity tests showed that none of them seemed to have much impact on SW (Figures 5e and 5h), while for LW, it was ERA5_INITIAL that contributed to the peak at approximately 280 W m^{-2} in ALL_TESTS, which was also apparent in the measurements (Figures 5f and 5i).

The above analysis of LWP PDFs showed that changing meteorological input fields from UKMO analysis to ERA5 (ERA5_INITIAL) especially contributed to the improved representation of LWP in ALL_TESTS compared with

CONTROL. To understand better the reasons for this and how the boundary layer structure in the initial conditions propagates to the model, Figure 6 compares potential temperature profiles from Met Office analysis and ERA5 (used for the initialization for each forecast cycle) with output 1 hour after the initialization from the CONTROL and ERA5_INITIAL experiments. Equivalent profiles of water vapor mixing ratio are shown in Figure S7 in Supporting Information S1. Also included in Figure 6 are the profiles of potential temperature from the radiosonde launches, which occurred at roughly the same time as the model output 1 hour after initialization. In general, the ERA5 output show a deeper mixed layer than the UKMO analysis, as well as better agreement with the radiosonde measurements. A deeper mixed layer implies more mixing in the boundary layer in ERA5_INITIAL relative to CONTROL. This would transport more water vapor from the surface to cloud level, and promote the condensation of liquid water in updrafts, that is, act to increase the formation of low-level liquid clouds in ERA5_INITIAL relative to CONTROL. This is also seen in the height of the top of the boundary layer as diagnosed by the UM, which is on average higher in ERA5_INITIAL than in CONTROL (Figure S8 in Supporting Information S1).

Table 3

Mean and Median Values of Downwelling SW and LW Fluxes in the Coastal Case Study (31st January 2018–5th February 2018) for Measurements, CONTROL, and Unified Model Sensitivity Tests

	Downwelling SW flux [W m^{-2}]		Downwelling LW flux [W m^{-2}]	
	Mean	Median	Mean	Median
CAPRICORN-2	146.14	93.17	268.22	277.29
CONTROL	257.48	163.66	244.69	248.37
FIXED_DROP	247.07	159.14	245.81	247.97
ICE_MICROPHYS	247.94	143.47	247.82	248.54
ERA5_INITIAL	248.77	159.38	247.63	260.33
MIXING	246.92	166.23	248.03	247.65
ALL_TESTS	227.59	126.76	250.45	262.85

Note. Bold values in each column indicate closest numerical agreement with observed value.

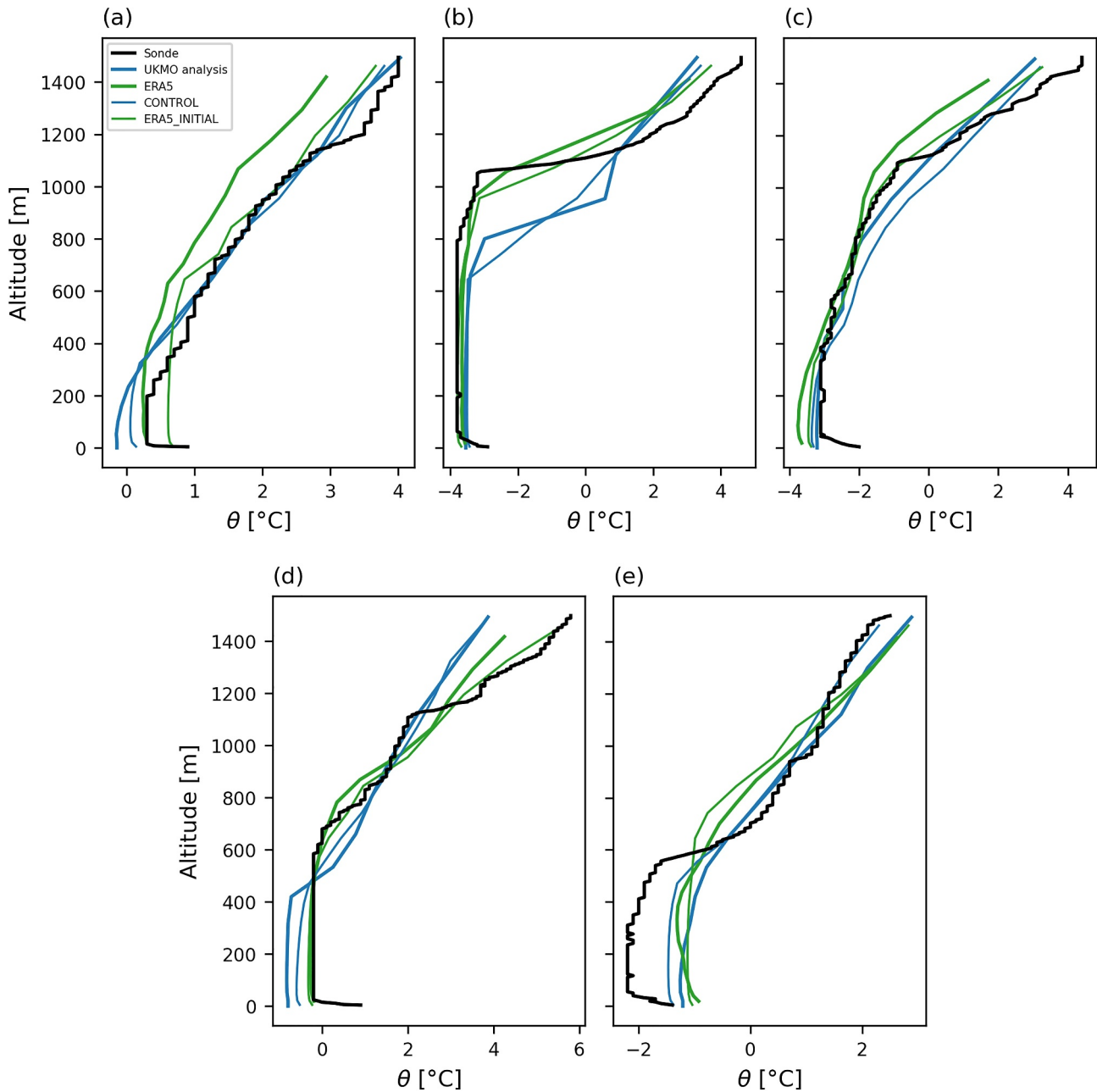


Figure 6. Vertical profiles of potential temperature at the time of model initialization (00:00 UTC) for each forecast of the coastal case study on (a) 31st January, (b) 1st February, (c) 2nd February, (d) 3rd February, and (e) 4th February. Profiles are from radiosondes (black lines), UKMO analysis initial condition fields (thick blue lines), and ERA5 initial condition fields (thin green lines). Also included are profiles from model output from 1 hr after initialization (01:00 UTC) from CONTROL (thin blue lines) and ERA5_INITIAL (thin green lines). Radiosonde releases were at (a) 01:05, (b) 00:53, (c) 00:53, (d) 00:59, and (e) 01:02 UTC on each day.

3.3. AMSR2 Comparison

In the previous section, the use of point measurements from the ship restricts the scope of our evaluation to a limited spatial extent. Therefore, Figure 7 compares estimates of LWP from the AMSR2 satellite with outputs from the CONTROL and ALL_TESTS simulations for the entire coastal case study model domain area (Figure 1). Like the CAPRICORN-2 measurements, the AMSR2 measurements show a left skewed distribution peaking at low values, and a maximum value of around 450 g m^{-2} . The PDF from CONTROL is displaced to the left compared with the measurements, with too many occurrences of low LWP values despite the maximum value of around 475 g m^{-2} being close to the maximum value of the measurements. By contrast, the PDF from

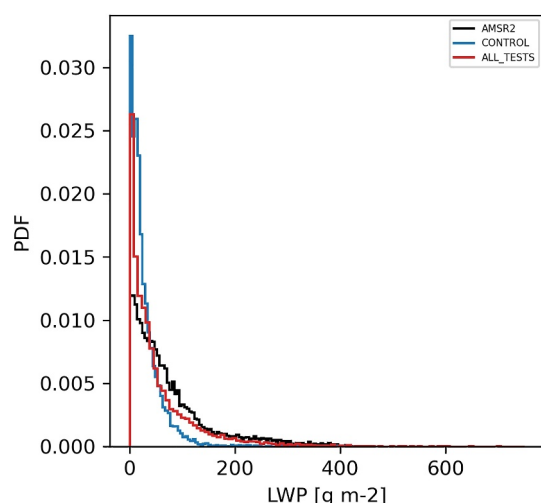


Figure 7. Probability density functions of liquid water path (LWP) from daily ascending and descending Advanced Microwave Scanning Radiometer 2 measurements of LWP (black) and corresponding output from the CONTROL (blue) and ALL_TESTS (red) simulations for the coastal case study (31st January 2018–5th February 2018). Results are over the entire coastal case study domain area. Note that only LWP values above 0.1 g m^{-2} are included.

ALL_TESTS is in better agreement with the measurements than CONTROL. However, compared with the measurements it is still somewhat left skewed, with a larger maximum value of about 750 g m^{-2} . The median LWP values for the AMSR2, CONTROL, and ALL_TESTS distributions shown in Figure 7 are 52.50, 18.83, and 31.93 g m^{-2} , respectively.

4. Discussion

The results presented in Section 3 provide several key insights into UM simulations of mixed-phase Southern Ocean clouds and their interactions with aerosols. We will now discuss the implications of the results.

4.1. Aerosols

The N_{10} concentration is underestimated in the CONTROL simulations for both model domains (Figure 2). The mean value in the CONTROL output is approximately an order of magnitude too low in the coastal case study, which perhaps suggests that possible biogenic sources of particles in the productive Antarctic coastal region (i.e., secondary particle formation from oxidation products of DMS) are not present in the model. This is unsurprising since our UM simulations do not include secondary new particle formation in the boundary layer. However, switching on boundary layer new particle formation in UKCA increases N_{10} concentration by approximately 60% at the surface (not shown), but this is not enough to account for the model bias, which still remains underestimated by approximately a factor of 5 when this

process is switched on. The concentration of DMS in the ocean and the associated emissions into the atmosphere are uncertain, with previous studies showing sensitivity of aerosol properties to the seawater DMS data set (Bhatti et al., 2023) or DMS chemistry scheme used (Revell et al., 2019). This is therefore another potential source of bias in our model results. UKCA is also missing the gas species methanesulfonic acid (MSA) that can also be formed from the oxidation of DMS and can play a role in the formation and growth of aerosol particles. Raised concentrations of MSA were measured near the coast during the CAPRICORN-2 campaign (McFarquhar et al., 2021). Thus, the absence of MSA in our model could also contribute to the underestimation of N_{10} in the biologically active coastal domain.

The N_{10} values from the CONTROL simulation are also an order of magnitude too low in the ocean case study, which is in a less biogenically productive region than the coastal case study, suggesting that biogenically driven new particle formation is not the only model process causing biases in N_{10} . Primary emission of aerosol from sea spray is also a key source in the Southern Ocean. Sea salt burdens have been shown to be highly uncertain in CMIP6 models, that is, a large inter-model spread (Lapere et al., 2023). Sea spray parameterizations typically depend on wind speed, sea surface temperature and/or salinity, but both the source functions and the size distributions used in such parameterizations are not well constrained (Grythe et al., 2014). The UKCA model uses the parameterization by Gong (2003), which has been shown by Regayre et al. (2020) to underestimate CCN in this region of the Antarctic coast compared to measurements from a different campaign. Regayre et al. (2020) also showed that parameters used in the calculation of aerosol dry deposition can have a significant influence on aerosol concentrations in this region, and that aerosol wet removal was too strong.

4.2. Cloud Liquid Water

We showed that LWP is particularly underestimated by CONTROL in the coastal case study (Figure 3). To investigate the cause of this, we undertook a set of sensitivity tests for this case study that focused on several key processes that control increases and decreases in cloud liquid water. We will discuss the findings in this section.

4.2.1. Liquid Removal Processes

The CONTROL simulation consistently underestimates CDNC (Figure 2). For a given amount of cloud liquid, low CDNC values are linked with larger droplet sizes, making the formation of rain droplets more efficient. Low CDNC is therefore associated with stronger removal of liquid water by precipitation. The use of fixed CDNC

values in FIXED_DROP allowed us to overcome the aerosol biases when simulating the cloud behavior to test this aerosol-precipitation feedback. However, the LWP in the coastal case study is mostly insensitive to the use of fixed CDNC, at least for the value used in the FIXED_DROP simulations (Figure 5). This is true both when clouds are present in the CONTROL simulation (e.g., 3rd February, Figure S3 in Supporting Information S1) and when CONTROL failed to simulate the presence of liquid cloud (e.g., 31st January). This insensitivity of LWP to CDNC suggests that the biases in the LWP are not purely a result of the aerosol biases in the model.

In addition to the use of a fixed CDNC value, sensitivity tests were carried out relating to the formation of ice in the UM. Since the clouds in the coastal domain are mixed-phase, the modeled ice formation processes can suppress liquid water via the Wegener-Bergeron-Findeisen process. We used two approaches to attempt to reduce the amount of ice in the model domain to investigate the Wegener-Bergeron-Findeisen effect, referred to as ICE_MICROPHYS. We prevented ice from entering the high-resolution regional domain from the driving model and we altered several model processes with the aim of making ice formation weaker. Note that these changes were intended as crude sensitivity tests, to investigate whether model biases related to the competition between liquid and ice phase cloud water is responsible in this case for the model underestimation of LWP, rather than physically motivated changes. However, there is a large degree of uncertainty in the parameterizations used to represent ice formation in clouds. Like the results from the FIXED_DROP simulation, the LWP distribution from the ICE_MICROPHYS simulation is broadly similar to that from CONTROL (Figure 5).

Overall, the UM is more sensitive to the ice from the lateral boundary conditions than it is to online modeled ice processes (not shown). This suggests that the large-scale forcing plays a role in the simulation of the clouds in the regional domain. However, it is important to remember that there is a complex array of processes controlling ice formation in the UM, and we have not comprehensively tested all of them here. Moreover, even after altering the lateral boundary conditions, significant biases remain in LWP, downwelling SW, and downwelling LW.

4.2.2. Sources of Liquid Water

After running tests in the coastal case study to investigate the model treatment of liquid water removal processes (autoconversion to rain in FIXED_DROP, loss to ice in ICE_MICROPHYS), biases seen in UM simulation CONTROL were still present. Thus, to try and eliminate the bias, we ran further tests targeting sources of liquid water.

In ERA5_INITIAL, we initialized the global driving UM model with ERA5 instead of the default UKMO analysis. The LWP output from simulation ERA5_INITIAL shows that extra moisture from the different initial conditions increase the modeled LWP on average (Figure 5 and Figure S4 in Supporting Information S1). ERA5 produces on average a deeper mixed layer than the UKMO analysis (Figure 6, Figures S7 and S8 in Supporting Information S1), which promotes cloud formation. This provides support for the theory that meteorological fields, rather than aerosol properties, are primarily the cause of biases in cloud properties in the UM regional domain. Moreover, the increased LWP sometimes improves the model-observation agreement in the downwelling LW flux (e.g., 31st January, Figure S6 in Supporting Information S1). However, at other times, biases remain, and overall the simulation of downwelling SW and LW is only slightly improved. Therefore, despite the improvements offered by using moister initial conditions, this change alone cannot provide a totally accurate simulation of the clouds in the UM during this period of the CAPRICORN-2 campaign.

Finally, simulation MIXING was run to test the effect of more boundary layer mixing on the liquid water content in the simulation, as this leads to greater vertical transport of water vapor from surface to cloud level, thus supplying more liquid water to the cloud via condensation. Like ERA5_INITIAL, improvements are seen in MIXING in output of LWP and the downwelling fluxes relative to CONTROL, though biases remain.

5. Conclusions

We have simulated two case studies from the CAPRICORN-2 field campaign in the Southern Ocean during austral summer 2018. Output from the regional UM model coupled to CASIM and UKCA shows that the aerosol concentration is underestimated at the surface, both in the open ocean at approximately 50°S, and in the biologically productive region near the Antarctic coast. The underestimation of aerosol concentration in both case studies suggests that the model is not able to capture the difference in aerosol source processes between the two regions. The modeled CDNC values are about an order of magnitude too low because of the aerosol bias. This

underestimation of surface aerosol concentration in our model merits further evaluation and model development. Marine aerosol sources in Antarctic sea ice regions hold particular importance since they represent a potentially important link in the Antarctic climate system between the atmosphere and the ocean. Thus, further study of aerosol processes for a range of sea ice conditions (i.e., in different seasons) is warranted, though the relative lack of observations outside of the summer season, or at cloud level, makes this difficult. Mass spectrometry results may help to investigate aerosol biases relating to specific species (e.g., sulfate), which could assist in highlighting specific processes that warrant further attention in the model, as well as affecting the activation efficiency of particles via their hygroscopicity. In addition, further analysis of the ocean open case may be an interesting topic of further work, since previous studies have highlighted the role of the free troposphere as a source of particles to the cloud level in the Southern Ocean (McCoy et al., 2021; Twohy et al., 2021).

We have assessed the impact of the aerosol bias on the modeled cloud microphysics and radiative properties. The impact appears to differ between regions. Near the Antarctic coast, the CAPRICORN-2 measured LWP is underestimated by the model by approximately 15 g m^{-2} or 32% (mean values). Surface downwelling SW flux is overestimated by approximately 111 W m^{-2} (76%) by the model, corresponding to the underestimation in LWP, while surface downwelling LW flux is somewhat overestimated. By contrast, the ocean region further north does not display the same biases, with much better model-observation agreement for LWP.

We have investigated the link between the aerosol and cloud biases in the coastal region. We ran simulations to conduct sensitivity tests that targeted processes that create or remove cloud liquid water in the model. We found that trying to weaken the (cloud microphysical) loss terms for liquid water only had a marginal effect on the LWP. Like the default configuration of the model, low values of LWP were overestimated and higher values underestimated. By contrast, simulations where we altered the meteorology in the simulations caused better agreement with the observed LWP. Using ERA5 for the initial conditions of the simulations increased mean LWP by approximately 45% and enhancing model boundary layer mixing increased LWP by about 29%. As such, more attention needs to be given to the temperature profile, boundary layer structure and the supply of moisture to the clouds. Thus, it appears that biases in meteorology are obscuring the coupling between aerosols and clouds in this region.

The effect on the downwelling surface SW flux from our sensitivity tests was less pronounced than the changes to LWP. The decrease in downwelling SW in individual sensitivity tests varied from about 3% to 6%, with the greatest reduction of 6% coming from the use of a fixed droplet number concentration. The limited mean SW response to individual tests is likely due to the day-to-day variability in the SW response in different simulations (Figure S5 in Supporting Information S1). In general, the greatest improvement in modeled LWP and downwelling SW flux was from our simulation with all sensitivity tests combined, which increased LWP by 47% and decreased downwelling SW by 10%. This improved model-observation agreement in our combined test potentially indicates some non-linearity between the effects of liquid sources and sinks on the cloud microphysical behavior. The same simulation also performs better than the model baseline when the distribution of modeled LWP is compared with that from satellite measurements, suggesting that the conclusions from the CAPRICORN-2 case studies may be more broadly relevant in this region. Note that in evaluating the surface radiative biases, we have only considered cloud radiative effects and have not considered any potential bias caused by the interaction of water vapor with longwave radiation, or direct interaction of aerosol particles with shortwave radiation. However, we are confident that due to the low aerosol optical depth (and by extension, low sensitivity of shortwave flux to aerosol) in this region (e.g., Mulcahy et al., 2018; Thorsen et al., 2020), any bias in surface shortwave flux due to aerosol direct effects would be small relative to the cloud radiative effects that we have investigated here.

Data Availability Statement

Aerosol concentrations measured using the condensation particle counter during CAPRICORN-2 (voyage IN2018_V01) are published on the CSIRO data portal at <https://doi.org/10.25919/2h1c-t753>. Downwelling radiative fluxes measured by pyranometer and pyrgeometer from CAPRICORN-2 are published on the CSIRO data portal with the underway data at https://www.marine.csiro.au/data/trawler/survey_details.cfm?survey=IN2018_V01 [last accessed 28-04-2024]. Radiosondes launched during voyage IN2018_V01 are published on the CSIRO portal at <https://doi.org/10.5065/D69P30HG>. Cloud droplet number concentration and liquid water path retrievals from CAPRICORN-2 will soon be available on the CSIRO data portal. Time series of UM output collocated with the R/V *Investigator* and two-dimensional liquid water path fields on AMSR2 grid are available

from <https://doi.org/10.5281/zenodo.13145408> along with Python code used to analyze the data and produce the figures. Owing to intellectual property rights restrictions, we cannot provide the source code or documentation papers for the UM. The Met Office UM is available for use under license. A number of research organizations and national meteorological services use the UM in collaboration with the Met Office to undertake basic atmospheric process research, produce forecasts, and develop the UM code. To apply for a license, see <http://www.metoffice.gov.uk/research/modelling-systems/unified-model>. CASIM is open source (BSD3 license) and it is available from code.metoffice.gov.uk, which requires registration.

Acknowledgments

We thank the editor, Yun Qian, and three anonymous reviewers for their valuable comments and suggestions, which have greatly improved the quality of this manuscript. Ruth Price, Andrew Orr, and Paul Field received support from the European Union's Horizon 2020 research and innovation framework programme under Grant agreement no. 101003590 (PolarRES). This work used JASMIN, the UK's collaborative data analysis environment (<https://www.jasmin.ac.uk>) and the ARCHER2 UK National Supercomputing Service (<https://www.archer2.ac.uk>). This project received grant funding from the Australian Government as part of the Antarctic Science Collaboration Initiative programme under the Australian Antarctic Program Partnership, ASCI000002. This research was supported by a Grant of sea time on RV *Investigator* from the CSIRO Marine National Facility (<https://ror.org/01mae9353>).

References

- Abdul-Razzak, H., & Ghan, S. (2000). A parameterization of aerosol activation 2. Multiple aerosol types. *Journal of Geophysical Research*, *105*(D5), 6837–6844. <https://doi.org/10.1029/1999jd901161>
- Barrett, A. I., Hogan, R. J., & Forbes, R. M. (2017). Why are mixed-phase altocumulus clouds poorly predicted by large-scale models? Part 2. Vertical resolution sensitivity and parameterization. *Journal of Geophysical Research: Atmospheres*, *122*(18), 9927–9944. <https://doi.org/10.1002/2016JD026322>
- Bhatti, Y. A., Revell, L. E., Schuddeboom, A. J., McDonald, A. J., Archibald, A. T., Williams, J., et al. (2023). The sensitivity of Southern Ocean atmospheric dimethyl sulfide (DMS) to modeled oceanic DMS concentrations and emissions. *Atmos. Chem. Phys.*, *23*(24), 15181–15196. <https://doi.org/10.5194/acp-23-15181-2023>
- Bodas-Salcedo, A., Mulcahy, J., Andrews, T., Williams, K., Ringer, M., Field, P., & Elsaesser, G. (2019). Strong dependence of atmospheric feedbacks on mixed-phase microphysics and aerosol-cloud interactions in HadGEM3. *Journal of Advances in Modeling Earth Systems*, *11*(6), 1735–1758. <https://doi.org/10.1029/2019MS001688>
- Boutle, I., Eyre, J., & Lock, A. (2014). Seamless stratocumulus simulation across the turbulent gray zone. *American Meteorological Society*, *142*(4), 1655–1668. <https://doi.org/10.1175/mwr-d-13-00229.1>
- Bush, M., Boutle, I., Edwards, J., Finnenkoetter, A., Franklin, C., Hanley, K., & Weeks, M. (2023). *The second Met Office Unified Model-JULES regional atmosphere and land configuration, RAL2* (Vol. 16, pp. 1713–1734). Copernicus Publications.
- Carslaw, K., Lee, L., Reddington, C., Pringle, K., Rap, A., Forster, P., et al. (2013). Large contribution of natural aerosols to uncertainty in indirect forcing. *Nature*, *503*(7474), 67–71. <https://doi.org/10.1038/nature12674>
- Ceppi, P., Hwang, Y., Frierson, D., & Hartmann, D. (2012). Southern Hemisphere jet latitude biases in CMIP5 models linked to shortwave cloud forcing. *Geophysical Research Letters*, *39*(19), 19708. <https://doi.org/10.1029/2012GL053115>
- Cesana, G., Khadir, T., Chepfer, H., & Chiriacco, M. (2022). Southern Ocean solar reflection biases in CMIP6 models linked to cloud phase and vertical structure representations. *Geophysical Research Letters*, *49*(22), e2022GL099777. <https://doi.org/10.1029/2022GL099777>
- Field, P., Hill, A., Shipway, B., Furtado, K., Wilkinson, J., Miltenberger, A., et al. (2023). Implementation of a double moment cloud microphysics scheme in the UK met office regional numerical weather prediction model. *Quarterly Journal of the Royal Meteorological Society*, *149*(752), 703–739. <https://doi.org/10.1002/qj.4414>
- Fitzpatrick, M., & Warren, S. (2007). The relative importance of clouds and sea ice for the solar energy budget of the Southern Ocean. *Journal of Climate*, *20*(6), 941–954. <https://doi.org/10.1175/jcli4040.1>
- Furtado, K., & Field, P. R. (2017). The role of ice microphysics parametrizations in determining the prevalence of supercooled liquid water in high-resolution simulations of a Southern Ocean midlatitude cyclone. *Journal of the Atmospheric Sciences*, *74*(6), 2001–2021. <https://doi.org/10.1175/jas-d-16-0165.1>
- Furtado, K., Field, P. R., Boutle, I. A., Morcrette, C. J., & Wilkinson, J. M. (2016). A physically based subgrid parameterization for the production and maintenance of mixed-phase clouds in a general circulation model. *Journal of the Atmospheric Sciences*, *73*(1), 279–291. <https://doi.org/10.1175/jas-d-15-0021.1>
- Gilbert, E., Orr, A., King, J., Renfrew, I., Lachlan-Cope, T., Field, P., & Boutle, I. (2020). Summertime cloud phase strongly influences surface melting on the Larsen C ice shelf, Antarctica. *Quarterly Journal of the Royal Meteorological Society*, *146*(729), 1575–1589. <https://doi.org/10.1002/qj.3753>
- Gong, S. (2003). A parameterization of sea-salt aerosol source function for sub- and super-micron particles. *Global Biogeochemical Cycles*, *17*(4). <https://doi.org/10.1029/2003gb002079>
- Gordon, H., Carslaw, K., Hill, A., Field, P., Abraham, N., Beyersdorf, A., et al. (2023). NUMAC: Description of the nested unified model with aerosols and chemistry, and evaluation with KORUS-AQ data. *Journal of Advances in Modeling Earth Systems*, *15*(11), e2022MS003457. <https://doi.org/10.1029/2022MS003457>
- Gordon, H., Field, P., Abel, S., Barrett, P., Bower, K., Crawford, I., et al. (2020). Development of aerosol activation in the double-moment Unified Model and evaluation with CLARIFY measurements. *Atmospheric Chemistry and Physics*, *20*(18), 10997–11024. <https://doi.org/10.5194/acp-20-10997-2020>
- Grosvenor, D., Field, P., Hill, A., & Shipway, B. (2017). The relative importance of macrophysical and cloud albedo changes for aerosol-induced radiative effects in closed-cell stratocumulus: Insight from the modelling of a case study. *Atmospheric Chemistry and Physics*, *17*(8), 5155–5183. <https://doi.org/10.5194/acp-17-5155-2017>
- Grythe, H., Ström, J., Krejci, R., Quinn, P., & Stohl, A. (2014). A review of sea-spray aerosol source functions using a large global set of sea salt aerosol concentration measurements. *Atmospheric Chemistry and Physics*, *14*(3), 1277–1297. <https://doi.org/10.5194/acp-14-1277-2014>
- Hansen, N., Orr, A., Zou, X., Boberg, F., Bracegirdle, T., Gilbert, E., & Webster, S. (2023). The importance of cloud phase when assessing surface melting in an offline coupled firn model over Ross Ice shelf. *West Antarctica*. <https://doi.org/10.5194/ta-2023-145>
- Hersbach, H., Bell, B., Berrisford, P., Hirahara, S., Horányi, A., Muñoz-Sabater, J., et al. (2020). The ERA5 global reanalysis. *John Wiley and Sons, Ltd*, *146*(730), 1999–2049. <https://doi.org/10.1002/qj.3803>
- Humphries, R., McRobert, I., Ward, J., Harnwell, J., & Keywood, M. (2020). *CAPRICORN2 - Atmospheric aerosol measurements from the RV Investigator voyage IN2018_V01*. v3. CSIRO. Data Collection. <https://doi.org/10.25919/2h1c-t753>
- Illingworth, A., Hogan, R., O'Connor, E., Bouniol, D., Brooks, M., Delanoë, J., & Wrench, C. (2007). Cloudnet: Continuous evaluation of cloud profiles in seven operational models using ground-based observations. *American Meteorological Society*, *88*(6), 883–898. Retrieved from <https://journals.ametsoc.org/view/journals/bams/88/6/bams-88-6-883.xml>
- Imaoka, K., Kachi, M., Kasahara, M., Ito, N., Nakagawa, K., & Oki, T. (2010). Instrument performance and calibration of AMSR-e and AMSR2.

- Kang, S., Ceppi, P., Yu, Y., & Kang, I. (2023). Recent global climate feedback controlled by Southern Ocean cooling. *Nature Geoscience* 2023, 16(9), 775–780. <https://doi.org/10.1038/s41561-023-01256-6>
- Kay, J., Wall, C., Yettella, V., Medeiros, B., Hannay, C., Caldwell, P., & Bitz, C. (2016). Global climate impacts of fixing the Southern Ocean shortwave radiation bias in the Community Earth System Model (CESM). *Journal of Climate*, 29(12), 4617–4636. <https://doi.org/10.1175/jcli-d-15-0358.1>
- Lang, F., Huang, Y., Protat, A., Truong, S., Siems, S., & Manton, M. (2021). Shallow convection and precipitation over the Southern Ocean: A case study during the CAPRICORN 2016 field campaign. *Journal of Geophysical Research: Atmospheres*, 126(9), e2020JD034088. <https://doi.org/10.1029/2020JD034088>
- Lapere, R., Thomas, J., Marelle, L., Ekman, A., Frey, M., Lund, M., et al. (2023). The representation of sea salt aerosols and their role in polar climate within CMIP6. *Journal of Geophysical Research: Atmospheres*, 128(6), e2022JD038235. <https://doi.org/10.1029/2022JD038235>
- Lock, A., Brown, A., Bush, M., Martin, G., & Smith, R. (2000). A new boundary layer mixing scheme. Part I: Scheme description and single-column model tests. *Monthly Weather Review*, 128(9), 3187–3199. [https://doi.org/10.1175/1520-0493\(2000\)128<3187:anblms>2.0.co;2](https://doi.org/10.1175/1520-0493(2000)128<3187:anblms>2.0.co;2)
- Mace, G., Benson, S., Sterner, E., Protat, A., Humphries, R., & Hallar, A. (2024). The association between cloud droplet number over the summer Southern Ocean and air mass history. *John Wiley and Sons, Ltd.*, 129(12), e2023JD040673. <https://doi.org/10.1029/2023JD040673>
- Mace, G., Protat, A., Humphries, R., Alexander, S., McRobert, I., Ward, J., et al. (2021). Southern Ocean cloud properties derived from CAPRICORN and MARCUS data. *Journal of Geophysical Research: Atmospheres*, 126(4), e2020JD033368. <https://doi.org/10.1029/2020JD033368>
- McCoy, I., Bretherton, C., Wood, R., Twohy, C., Gettelman, A., Bardeen, C., & Toohey, D. (2021). Influences of recent particle formation on Southern Ocean aerosol variability and low cloud properties. *Journal of Geophysical Research: Atmospheres*, 126(8), e2020JD033529. <https://doi.org/10.1029/2020JD033529>
- McCusker, G., Vüllers, J., Achtert, P., Field, P., Day, J., Forbes, R., et al. (2023). Evaluating Arctic clouds modelled with the Unified model and integrated forecasting system. *Atmospheric Chemistry and Physics*, 23(8), 4819–4847. <https://doi.org/10.5194/acp-23-4819-2023>
- McFarquhar, G., Bretherton, C., Marchand, R., Protat, A., DeMott, P., Alexander, S., et al. (2021). Observations of clouds, aerosols, precipitation, and surface radiation over the Southern Ocean: An overview of CAPRICORN, MARCUS, MICRE, and SOCRATES. *Bulletin of the American Meteorological Society*, 102(4), E894–E928. <https://doi.org/10.1175/bams-d-20-0132.1>
- Morrison, A., Singh, H., & Rasch, P. (2022). Observations indicate that clouds amplify mechanisms of Southern Ocean heat uptake. *Journal of Geophysical Research: Atmospheres*, 127(4), e2021JD035487. <https://doi.org/10.1029/2021JD035487>
- Mulcahy, J., Jones, C., Sellar, A., Johnson, B., Boutle, I., Jones, A., et al. (2018). Improved aerosol processes and effective radiative forcing in HadGEM3 and UKESM1. *Blackwell Publishing Ltd*, 10(11), 2786–2805. <https://doi.org/10.1029/2018ms001464>
- O'Connor, F., Johnson, C., Morgenstern, O., Abraham, N., Braesicke, P., Dalvi, M., et al. (2014). Evaluation of the new UKCA Climate-Composition Model-Part 2: The troposphere. *Geoscientific Model Development*, 7(1), 41–91. <https://doi.org/10.5194/gmd-7-41-2014>
- O'Dell, C. W., Wentz, F. J., & Bennartz, R. (2008). Cloud liquid water path from satellite-based passive microwave observations: A new climatology over the global oceans. *Journal of Climate*, 21(8), 1721–1739. <https://doi.org/10.1175/2007JCLI1958.1>
- Protat, A., Schulz, E., Rikus, L., Sun, Z., Xiao, Y., & Keywood, M. (2017). Shipborne observations of the radiative effect of Southern Ocean clouds. *Journal of Geophysical Research: Atmospheres*, 122(1), 318–328. <https://doi.org/10.1002/2016JD026061>
- Regayre, L., Schmale, J., Johnson, J., Tatzelt, C., Baccarini, A., Henning, S., et al. (2020). The value of remote marine aerosol measurements for constraining radiative forcing uncertainty. *Atmospheric Chemistry and Physics*, 20(16), 10063–10072. <https://doi.org/10.5194/acp-20-10063-2020>
- Revell, L., Kremser, S., Hartery, S., Harvey, M., Mulcahy, J., Williams, J., et al. (2019). The sensitivity of Southern Ocean aerosols and cloud microphysics to sea spray and sulfate aerosol production in the HadGEM3-GA7.1 chemistry-climate model. *Atmospheric Chemistry and Physics Discussions*, 19(24), 1–36. <https://doi.org/10.5194/acp-19-15447-2019>
- Schmale, J., Baccarini, A., Thurnherr, I., Henning, S., Efraim, A., Regayre, L., et al. (2019). Overview of the Antarctic circumnavigation expedition: Study of preindustrial-like aerosols and their climate effects (ACE-SPACE). *Bulletin of the American Meteorological Society*, 100(11), 2260–2283. <https://doi.org/10.1175/bams-d-18-0187.1>
- Smagorinsky, J. (1963). General circulation experiments with the primitive equations. *Monthly Weather Review*, 91(3), 99–164. [https://doi.org/10.1175/1520-0493\(1963\)091%3C0099:GCEWTP%3E2.3.CO;2](https://doi.org/10.1175/1520-0493(1963)091%3C0099:GCEWTP%3E2.3.CO;2)
- Stanford, M., Fridlind, A., Silber, I., Ackerman, A., Cesana, G., Mühlensstädt, J., et al. (2023). Earth-system-model evaluation of cloud and precipitation occurrence for supercooled and warm clouds over the Southern Ocean's Macquarie Island. *Atmospheric Chemistry and Physics*, 23(16), 9037–9069. <https://doi.org/10.5194/acp-23-9037-2023>
- Thorsen, T., Ferrare, R., Kato, S., & Winker, D. (2020). Aerosol direct radiative effect sensitivity analysis. *American Meteorological Society*, 33(14), 6119–6139. <https://doi.org/10.1175/jcli-d-19-0669.1>
- Trenberth, K., & Fasullo, J. (2010). Simulation of present-day and twenty-first-century energy budgets of the Southern Oceans. *Journal of Climate*, 23(2), 440–454. <https://doi.org/10.1175/2009jcli3152.1>
- Twohy, C., DeMott, P., Russell, L., Toohey, D., Rainwater, B., Geiss, R., et al. (2021). Cloud-nucleating particles over the Southern Ocean in a changing climate. *John Wiley and Sons, Ltd*, 9(3), e2020EF001673. <https://doi.org/10.1029/2020EF001673>
- Van Weverberg, K., Morcrette, C. J., Boutle, I., Furtado, K., & Field, P. R. (2021). A bimodal diagnostic cloud fraction parameterization. Part I: Motivating analysis and scheme description. *Monthly Weather Review*, 149(3), 841–857. <https://doi.org/10.1175/MWR-D-20-0224.1>
- Vergara-Temprado, J., Miltenberger, A., Furtado, K., Grosvenor, D., Shipway, B., Hill, A., et al. (2018). Strong control of Southern Ocean cloud reflectivity by ice-nucleating particles. *Proceedings of the National Academy of Sciences of the United States of America* (Vol. 115(11)), 2687–2692. <https://doi.org/10.1073/pnas.1721627115>
- Vignon, E., Alexander, S., DeMott, P., Sotiropoulou, G., Gerber, F., Hill, T., et al. (2021). Challenging and improving the simulation of mid-level mixed-phase clouds over the high-latitude Southern Ocean. *Journal of Geophysical Research: Atmospheres*, 126(7), e2020JD033490. <https://doi.org/10.1029/2020JD033490>
- Wentz, F. J. (1997). A well-calibrated ocean algorithm for special sensor microwave/imager. *Journal of Geophysical Research*, 102(C4), 8703–8718. <https://doi.org/10.1029/96JC01751>
- Williams, R., Ceppi, P., Roussenov, V., Katavouta, A., & Meijers, A. (2023). The role of the Southern Ocean in the global climate response to carbon emissions. *Philosophical Transactions of the Royal Society A*, 381(2249). <https://doi.org/10.1098/rsta.2022.0062>
- Young, G., Lachlan-Cope, T., O'Shea, S., Dearden, C., Listowski, C., Bower, K., et al. (2019). Radiative effects of secondary ice enhancement in coastal Antarctic clouds. *Geophysical Research Letters*, 46(4), 2312–2321. <https://doi.org/10.1029/2018GL080551>
- Zelinka, M., Myers, T., McCoy, D., Caldwell, P., Ceppi, P., Klein, S., & Taylor, E. (2020). Causes of higher climate sensitivity. In *CMIP6 models*.